Simulation Study of Microwave Heating with Nanoparticle Diffusion for Tumor Ablation

Kazi Mahdi Mahmud, Md. Maruf Hossain Shuvo*

Department of Electronics and Communication Engineering
Khulna University of Engineering & Technology
Khulna-9203, Bangladesh
E-mails: utsha536@gmail.com, maruf.shuvo@ece.kuet.ac.bd

**Corresponding author*

Received: March 10, 2018 **Accepted: April 19, 2019**

Published: December 31, 2019

Abstract: *Microwave heating is one of the prominent treatment procedure that elevates body temperature using microwave energy to damage tumor cells. However, healthy tissues can also absorb microwave energy causing undesired damage. This research study focuses on optimizing the surrounding healthy tissue damage by diffusing magnetic nanoparticles (NPs) in the tumor region. A rectangular liver tissue is modeled using Finite Element Methods (FEM) and then a half-elliptical shaped tumor is incorporated in the model. A coaxial antenna covered with a polytetrafluoroethylene catheter is inserted at the edge of the liver tissue. Then the magnetic NPs are diffused within the tumor region. The performance of microwave heating with and without nanoparticle diffusion is compared using the performance parameters: power dissipation density, temperature distribution, and resultant tissue necrosis. Simulation results show that the heating procedure coupled with ferromagnetic nanoparticle diffusion has approximately 14% less damage to the healthy tissue. The study also shows that 433/915 MHz frequency value provides 3% less damage to the healthy tissue than 2.45 GHz. Analyzing the performance of different nanoparticle we found that the ferromagnetic nanoparticle provides 15% and 5% less damage to the healthy tissue than gold and manganese iron oxide NPs respectively. The obtained result was also verified for kidney, breast, and lung tumor ablations to confirm the findings.*

Keywords: *Microwave hyperthermia, Magnetic nanoparticle, Tumor necrosis, Liver tumor ablation, Finite element analysis.*

Introduction

The common treatments for cancer are surgical tumor removal, radiation therapy, and chemotherapy. In spite of being effective, these treatments are far from ideal. Surgical tumor removal is extremely invasive, while chemo and radiation therapies have the potentiality to cause serious side effects. Thus, there is an increasing demand for treatment procedure that is effective but minimizes invasiveness and undesirable side effects. The treatments that can meet these requirements involve mechanisms for specifically targeting cancer cells while keeping healthy tissues unaffected. One technique for specifically targeting tumors that have gained popularity due to its economic feasibility and minimal side effects is the thermal therapy. The thermal therapy that applies extreme heat to the tumor with the intention of killing all the malignant tissue is known as hyperthermia [14].

The limitation of hyperthermia therapy is that patients experience local pain and discomfort as well as while heating the tumor tissue for destruction, some surrounding healthy tissues are also damaged [15]. Thus, the temperature increase needs to be controlled to a specific region so that the damage to the normal tissue is minimized [5]. Several methods have been developed to localize electromagnetic radiation and its subsequent heating to the tumor. One of the prominent

methods is inserting a microwave-emitting probe directly into the tumor [2]. Another proven method of localization is injecting magnetic nanoparticles into the tumor, which then excited with microwave radiation [13]. In this study, we will examine the effect of these two localization strategies.

Mild hyperthermia treatments (40-43 °C) induce heat shock and cause changes in the cell cycle that lead to faster denaturation of the pathogenic cells. Temperatures of 43 °C and above allow for necrosis, or direct cell death adding the benefit of fully killing some tumor tissues [10]. Temperatures above 50 °C cause coagulation and temperatures of 60-90 °C results in thermoablation. Temperatures above 100 °C cause vaporization and anything around 200 °C results in tissue charring [8].

During the ablation procedure, an antenna is inserted into the target tissue that radiates electromagnetic energy at the microwave frequencies. Most currently available devices operate within the frequency bands approved for industrial, scientific, and medical (ISM) use, centered at 433 MHz, 915 MHz and 2.45 GHz [7]. Conventional microwave ablation antennas are coaxial antenna having axially symmetric radiation patterns [16]. Electromagnetic energy radiated from the antenna is deposited in the lossy tissue leading to heating via dielectric hysteresis. While thermal damage following ablation is a complex function of the time-temperature history during heating, temperatures in excess of 60 °C lead to near instantaneous cell death. A fundamental principle of successful ablation is the creation of an ablation zone that sufficiently covers the entire tumor and margin of healthy tissue providing a margin of safety for adjacent structures.

There are many constituents of NPs, such as gold, silver, carbon nanotubes, fullerenes, manganese oxide, lipids, and micelles [3]. Magnetic iron oxide nanoparticles (IONPs) are highly used for diagnostic and therapeutic agents because of low cost, tunable properties and biocompatibility [1]. Since the sizes of nanoparticles are smaller than or comparable to those of cells, it is easier for nanoparticles to get close to the targets. When exciting with an external magnetic field, the NPs generate localized heat that can be exploited for therapeutic hyperthermia treatment of tumors [11].

Our model consists of a liver tissue mimicking phantom containing a tumor and a coaxial antenna at the edge. At first, hyperthermia is induced by microwave heating initiated by the coaxial antenna probe at which the microwave input power is fed. After that, ferromagnetic nanoparticles are diffused within the tumor region using transport of diluted species physics domain and microwave heating is coupled to induce hyperthermia. The performance evaluation parameters: power dissipation density, temperature distribution, and resultant tissue necrosis are observed for both microwave heating with and without nanoparticle diffusion. Furthermore, the same simulation is carried out by varying the microwave frequency and using different nanoparticles.

Through comparative analysis, our study confirms that the most effective frequency is 433/915 MHz and the magnetic nanoparticle shows superior performance in minimizing damage to healthy tissue compared to other NPs. We performed the same analysis on kidney, breast and lung tissue mimicking phantoms and observed the similar performance in the nanoparticle-mediated hyperthermia. In this study, we performed the simulation in COMSOL Multiphysics (COMSOL Inc., ver. 5.2a) environment.

Materials and methods

Model definition

In this study, the problem domain consists of a liver tissue, a tumor, and a coaxial antenna. Firstly, we built the geometry for liver with a rectangle of 80 mm height and 30 mm wide as shown in Fig. 1. A half-elliptical shaped tumor of a) semiaxis 0.012 m, and b) semiaxis 0.015 m was incorporated at the left edge of the liver.

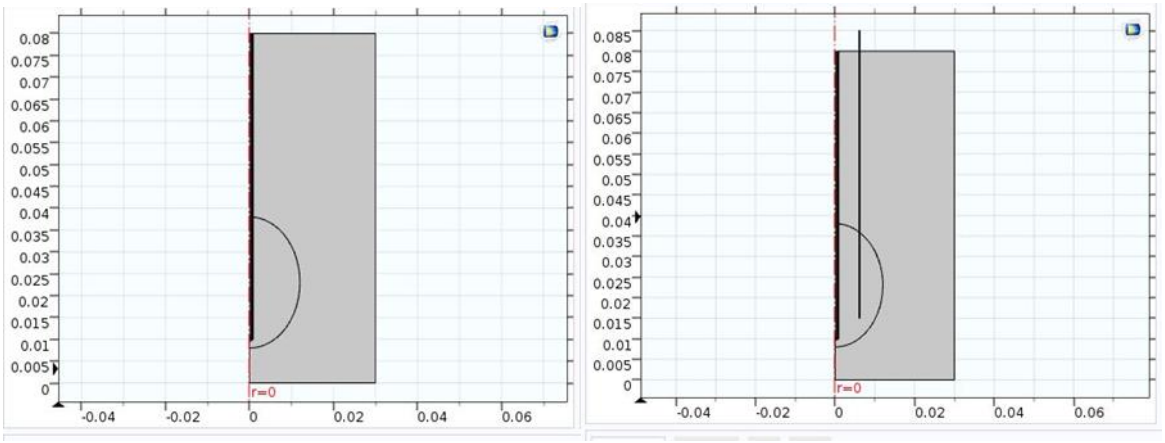

a) b)

Fig. 1 Geometry of liver tissue with the tumor for (a) microwave heating without NPs; (b) microwave heating coupled with NP diffusion.
Horizontal and vertical axis represents the domain dimension in meterc.

The rectangle in Fig. 1a presents liver tissue and the black line at the left edge represent the coaxial antenna while the half-elliptical shaped portion is the tumor. The polyvinyl chloride pipe is inserted into the tumor for nanoparticle transportation as shown in Fig. 1b. The coaxial cable is excited with a microwave input power of 10 W at the feed point. Due to this excitation, an electromagnetic wave propagated in the coaxial cable. This electromagnetic heating distributed temperature in the biological tissue through bio-heat transfer. The tissues and tumors are defined in using the parameters given in Table 1 [2, 6, 12]. The physical properties of the materials involved in the model are shown in Table 2 [3, 17].

Table 1. Different tissue and tumor properties in human

Tissue / Tumor	Electrical conductivity, (S/m)	Relative permittivity	Thermal conductivity, (W/mK)	Density, (kg/m^3)	Specific heat capacity, (J/kgK)
Liver	1.69	43.03	0.56	1040	3540
Liver tumor	2.00	45.00	0.60	1160	3540
Kidney	2.43	52.74	0.539	1050	3980
Kidney tumor	3.00	54.00	0.60	1120	3980
Breast	0.59	4.49	0.37	980	2960
Breast tumor	1.10	5.00	0.43	1060	2960
Lung	2.50	20.50	0.302	260	2560
Lung tumor	3.00	23.0	0.310	350	2560

In this study we have used a single thin coaxial antenna for microwave heating shown in Fig. 2. It is composed of an inner conductor, a dielectric and an outer conductor [9]. The main part of the antenna is a thin coaxial cable. The antenna has a ring-shaped slot of 1 mm cut on the outer

conductor and is 5.5 mm away from the short-circuited tip. The antenna enclosed in a sleeve catheter made of polytetrafluoroethylene is inserted from the left edge directly into the tumor. It can be operated at different ISM band frequencies like 433 MHz, 915 MHz, and 2.4 GHz. The microwave power input at the feeding point is 10 W. In the antenna the electromagnetic wave propagates in Transverse Electromagnetic fields (TEM) while in the liver tissue, the electromagnetic wave is characterized by the Transverse Magnetic fields (TM) [6].

Table 2. Parameter values used in the development of the model

Description	Value	Description	Value
Density of blood	1E3 kg/m^3	Input microwave power	10 W
Specific heat of blood	3639 J/(kgK)	Specific heat of liver	3500 J/(kgK)
Blood perfusion rate	3.6E-3 1/s	Density of liver	1050 kg/m^3
Blood temperature	37 °C	Nanoparticle volume	6.5450E-23 m^3
Relative permittivity of liver	43.03	Initial temperature everywhere	310.15 K
Electric conductivity of liver	1.69 S/m	Real permittivity of nanoparticles at 25% volume fraction	5.5
Thermal conductivity of liver	0.56 W/(mK)	Imaginary permittivity of nanoparticles at 25% volume fraction	0.7
Relative permittivity of dielectric	2.03	Real permeability of nanoparticles at 25% volume fraction	1.5
Relative permittivity of catheter	2.6	Imaginary permeability of nanoparticles at 25% volume fraction	0.7
Microwave frequency	2.45 GHz	Volume fraction	6.55E-5

Magnetic nanoparticles are transported to the tumor region through the polyvinyl chloride pipe which is inserted right into the tumor and the nanoparticles disperse within the tumor over time through mass transfer. We defined six cut points to visualize the effects of microwave heating in different regions which is shown in Fig. 3. The first three points are inside the tumor region and the rest are within the healthy tissue region.

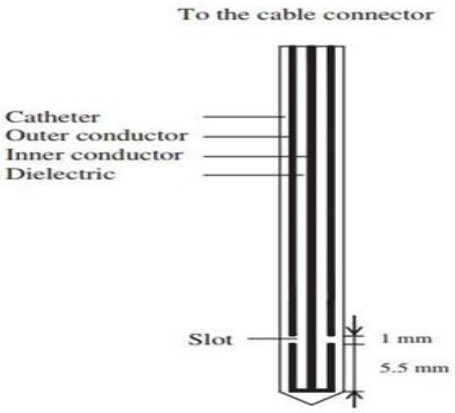

Fig. 2 Single coaxial antenna for microwave heating

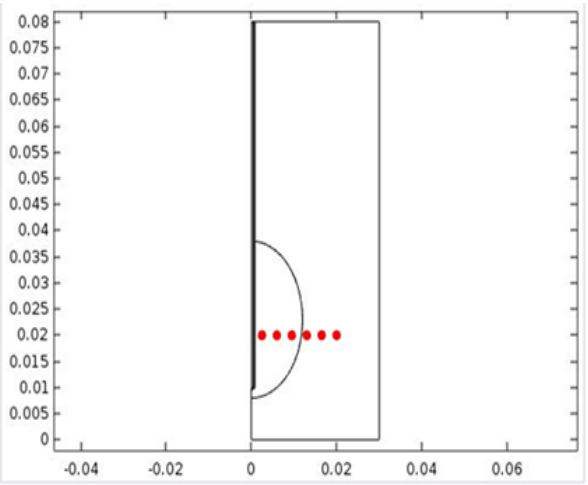

Fig. 3 Cut points

Domain and boundary equations

The electromagnetic wave in coaxial cable is denoted by TEM. The governing equations [2] are:

$$E = e_r \frac{C}{r} e^{j(\omega t - kz)}, \tag{1}$$

$$H = e_\varphi \frac{C}{z} e^{j(\omega t - kz)}, \tag{2}$$

$$P_{av} = \int_{r_{inner}}^{r_{outer}} \mathrm{Re}\left(\frac{1}{2} E \times H^*\right) 2\pi r dr = e_z \pi \frac{C^2}{Z} \ln\left(\frac{r_{outer}}{r_{inner}}\right), \tag{3}$$

where C represents amplitude and ω denotes the angular frequency. Here, z is the propagation direction and r, φ, z are cylindrical coordinates centered on the coaxial cable axis. Z is the wave impedance in the dielectric, while r_{inner} and r_{outer} is the dielectric's inner and outer radius respectively.

The electric and magnetic field flowing in the coaxial cable are defined in Eqs. (1) and (2) respectively. Eq. (3) is the time-averaged power flow P_{av} in cable. The relation between propagation constant, k, and the wavelength in the medium, λ, and is shown using Eq. (4):

$$k = \frac{2\pi}{\lambda}. \tag{4}$$

In the tissue, the electric field also has a finite axial component whereas the magnetic field is purely in the azimuthal direction. Thus, the model antenna uses an axisymmetric transverse magnetic (TM) formula as in Eq. (5). The wave equation becomes scalar

$$\nabla \times \left(\left(\frac{1}{\varepsilon_r - \frac{j\sigma}{\omega \varepsilon_0}} \right) \nabla \times H_\varphi \right) - \mu_r k_0^2 H_0, \tag{5}$$

where, σ is the electric conductivity, μ represents dielectric permeability and ε is dielectric permittivity. The electric field E is obtained from the Maxwell equations (Ampère's law) and the magnetic field H is solved from Eq. (5). The subscript 0 of a quantity represents the value of that quantity in the free space, and the subscript r represents the relative value (ratio) of that quantity to the free space value.

Let n denotes the unit normal vector for a surface. Then $n \times E = 0$ shows the boundary conditions for the metallic surfaces. A first-order low-reflecting boundary condition is used at outer boundaries of tissue which is shown in Eq. (7):

$$n \times \sqrt{\varepsilon} E - \sqrt{\mu} H_\varphi = -2\sqrt{\mu} H_{\varphi_0}. \tag{7}$$

Eq. (8) defines the input field at the coaxial cable port. The power level is set to 10 W.

$$H_{\varphi_0} = \frac{\sqrt{\frac{P_{av}Z}{\pi r \ln\left(r_{outer}/r_{inner}\right)}}}{r}. \tag{8}$$

The antenna radiates into the tissue and a damping wave propagates. The bio-heat equation at (9) describes the stationary heat transfer problem as:

$$\rho C_b \frac{\partial T}{\partial t} + \nabla\left(-k\nabla T\right) = \rho_b C_b \omega_{b(T_b - T)} + Q_{met} + Q_{ext}, \tag{9}$$

where k represents the liver's thermal conductivity (W/(m.K)); ρ_b – blood density (kg/m^3); C_b – blood's specific heat capacity (J/(kg.K)); ω_b – blood perfusion rate (1/s); Q_{met} – heat source from metabolism, and Q_{ext} – external heat source, both measured in W/m^3. This model neglects the heat source from metabolism.

Eq. (10) presents the external heat source which is the resistive heat generated by the electromagnetic field:

$$Q_{ext} = \frac{1}{2}\mathrm{Re}\left[\left(\sigma - j\omega\varepsilon\right)EE^*\right]. \tag{10}$$

Mass transfer of the nanoparticles throughout the tissue after needle injection can be modeled as a transient process, with the governing equations simplified as in Eq. (11):

$$\frac{\partial c_i}{\partial t} + \left(-D_i\nabla c_i\right) = R_i, \tag{11}$$

where c_i is the nanoparticle concentration (mole/m^3), D_i – diffusivity (m^2/s) of the nanoparticles through the tissue; R_i – reaction rate expression (mole/m^{3}s) for the species.

Results analysis and discussions

Fig. 4 depicts the transportation mechanism of magnetic nanoparticles. They are injected from the top of the injection pipe and released at the bottom of the pipe.

NPs spreads throughout the tumor region where their concentration is 1.661E-6 mole/m^3. Fig. 5a and Fig. 5b shows the distribution of the source power before and after injecting NPs respectively. Before injecting NPs some portion of the strong source power is seen to be dissipated outside the tumor region resulting in a strong electromagnetic field and high-temperature distribution. It is evident that the strong electromagnetic field is concentrated inside the tumor region after diffusing NPs. Hence, a higher temperature distribution is observed inside the tumor region than the healthy tissue region.

Fig. 6 shows the resulting steady-state temperature distribution before and after injecting NPs in the liver tissue for an input microwave power of 10 W. We observed that near the antenna, the heat source is strong, which leads to high temperatures as depicted in Fig. 6a, while far from the antenna, the heat source is weaker and the normal body temperature of 37 °C is maintained. Fig. 6b shows that the nanoparticles are effectively blocking the passage of energy into the tissue area. Therefore, around the nanoparticle site, almost 3-4 °C low temperature is monitored. This phenomenon indicates that the NPs are absorbing the microwave radiation.

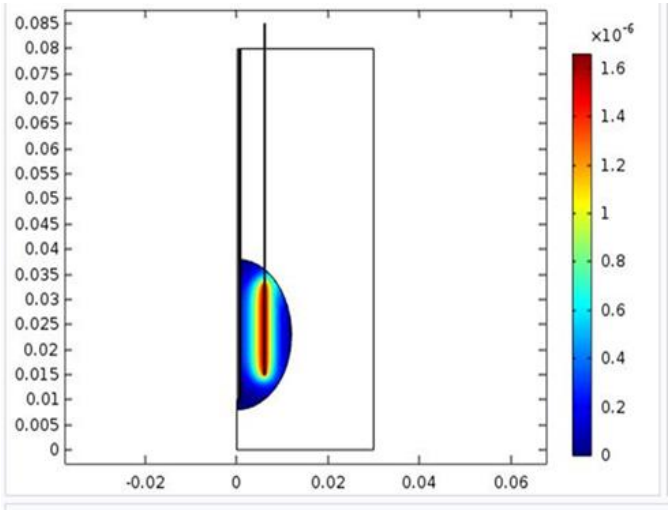

Fig. 4 Diffusion of magnetic nanoparticles in the tumor. The horizontal and vertical axes present the model dimension in meter and the sidebar shows different concentration values.

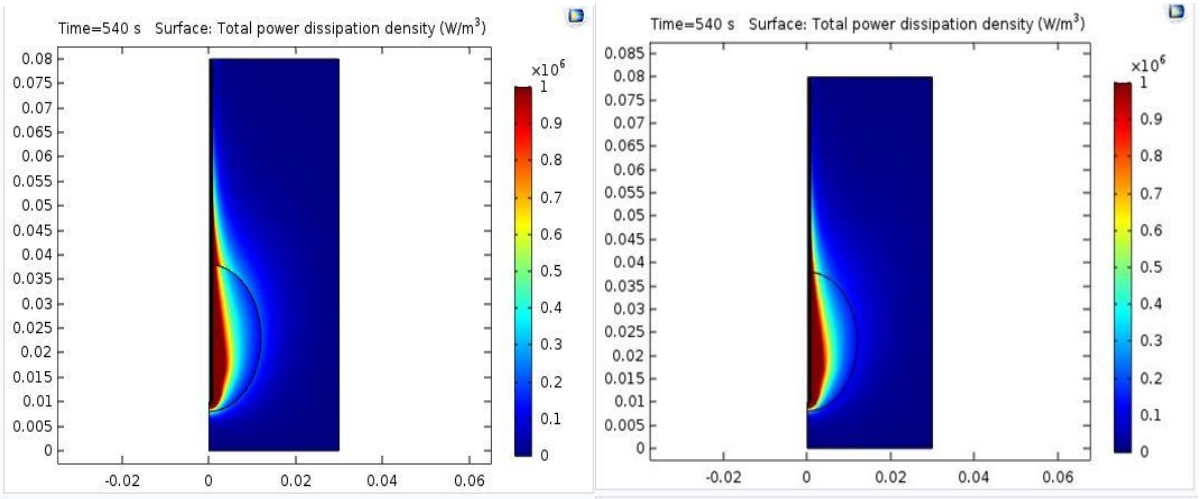

a) b)

Fig. 5 Power dissipation density: a) before injecting nanoparticles; b) after injecting nanoparticles. The horizontal and vertical axis are tissue dimensions in meter and the sidebar represents the strength of the electromagnetic field.

Fig. 7 shows the isothermal contour which presents the temperature at different regions of the tissue. To minimize the damage of healthy tissues, the body temperature should be kept below 43 °C. From Fig. 7a and Fig. 7b it is clear that away from the tumor domain temperature decreases from 42 to 38 °C for both the cases.

So, the suitable temperature for healthy tissues is maintained. It is clear that when NPs are not present in the computational domain, temperatures rise up to 53.79 °C in the tumor region and also a temperature of 47.13 °C rises beside and below the tumor domain. When NPs are present, high temperatures are within the tumor region and affect a small portion of the healthy tissue.

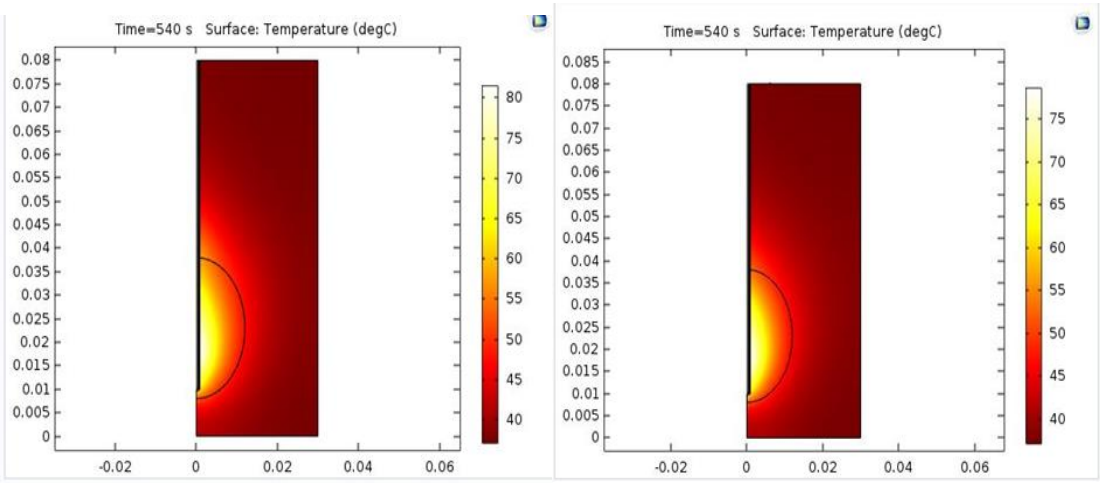

a) b)

Fig. 6 Temperature distribution: a) before injecting nanoparticles; b) after injecting nanoparticles. The horizontal and vertical axes are tissue dimensions in meter and the sidebar represents temperature in °C.

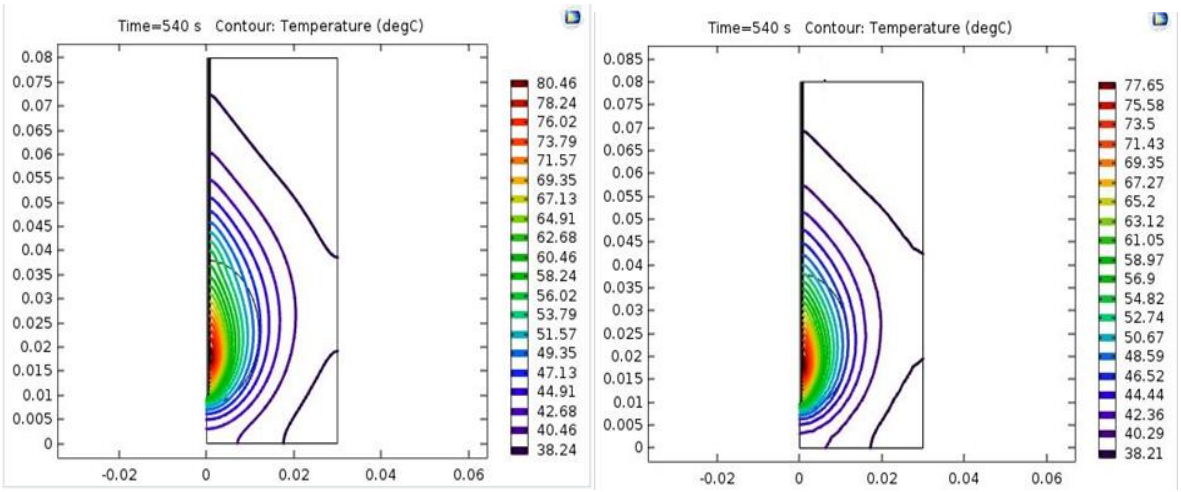

a) b)

Fig. 7 Isothermal contour: a) before injecting nanoparticles; b) after injecting nanoparticles. The horizontal and vertical axes are tissue dimensions in meter and the sidebar represents 20 different temperature values indicated by different colors.

Fig. 8 shows the fraction of necrotic tissue resulting from the microwave heating. When NPs are not present a noticeable portion of healthy tissue is damaged around the tumor region. On the other hand in the presence of NPs, a small portion of healthy tissue is damaged.

Fig. 9 represents how much of the tissue is damaged over time in different regions defined in the cut points. The blue curve corresponds to the innermost point's necrosis and the yellow one corresponds to the outermost point's necrosis.

Considering Fig. 9a and Fig. 9b, we observed that the tumor cell is almost destroyed for both the cases. In case of nanoparticle diffusion, it took a little bit long time. Observing the curves, we found that microwave heating alone hampers 69% of the healthy tissue. In contrast, when heating is combined with magnetic NPs only 55% of the healthy tissue is hampered. Away from the tumor less the difference is very acute. The same scenario observed in the vertical direction also.

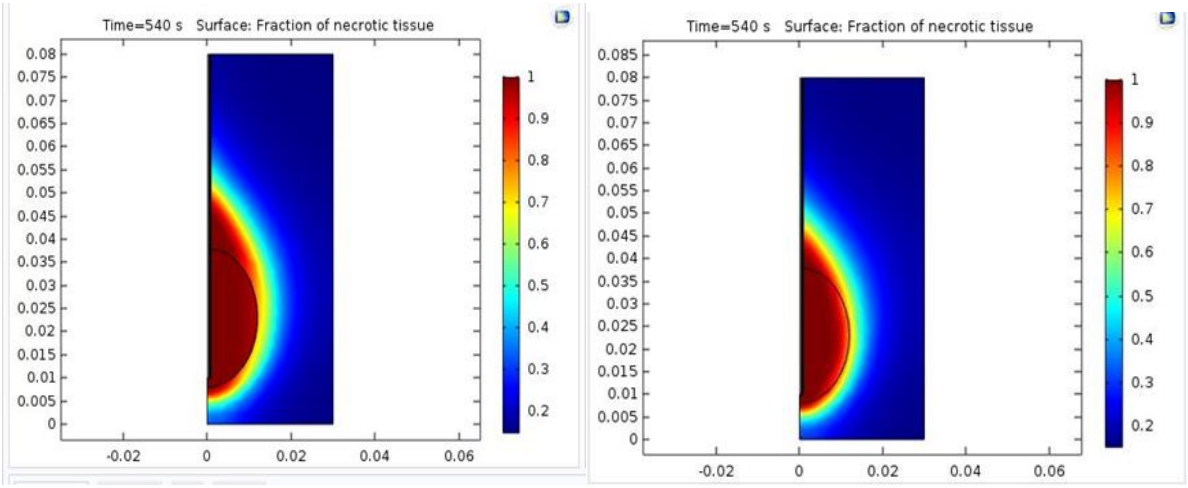

a) b)

Fig. 8 Fraction of necrotic tissue: a) before injecting nanoparticles; b) after injecting nanoparticles. The horizontal and vertical axes are tissue dimensions in meter and the sidebar represents how much portion of the tissue is damaged (1 dictates 100% damage).

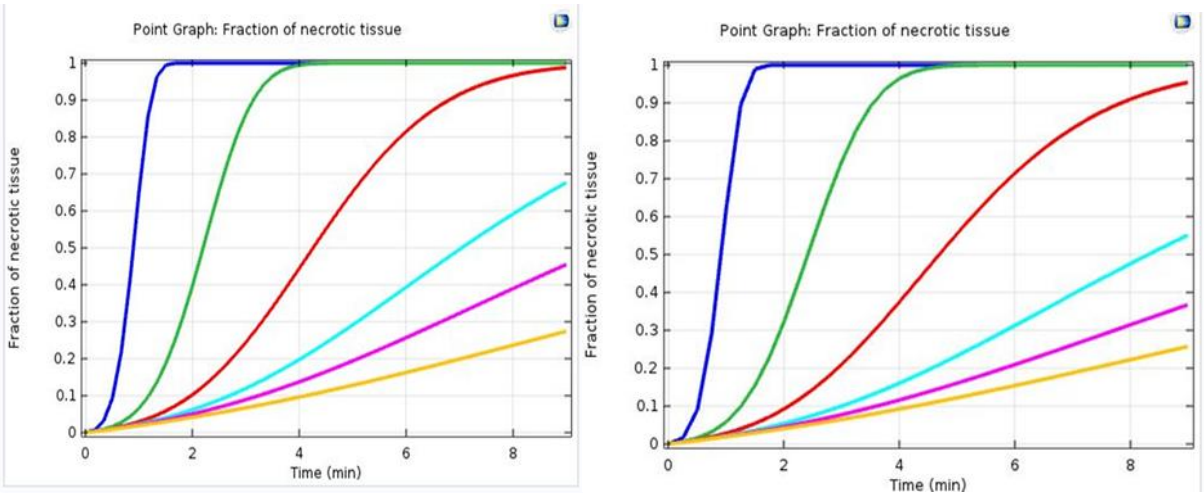

a) b)

Fig. 9 Point graph for damaged tissue: a) before injecting nanoparticles; b) after injecting nanoparticles. The horizontal axis represents treatment time in the minute and the vertical axis represents the portion of tissue necrosis due to heating (1 represents 100% necrosis).

Fig. 10 represents how much of the tissue is damaged at the 433/915 MHz frequency over time in the cut points. We observed that at 433/915 MHz the tumor damage decreased from 95% to 93% compared to the 2.45 GHz. On the other hand, the healthy tissue damage decreased from 55% to 52%. So, in this case, the healthy tissue damage around the tumor site decreased by 3%. Therefore, 433/915 MHz frequency would be more effective in minimizing healthy tissue damage around the tumor site for magnetic nanoparticle hyperthermia.

We observed the effects of different NPs for liver tumor ablation using microwave radiation. Fig. 11a and Fig. 11b shows the performance analysis of different NPs for liver tumor ablation in terms of percent damage versus time. In case of gold NP no significant improvement achieved in minimizing healthy tissue damage compared to the ferromagnetic NPs. Only 2% less damage is monitored around the tumor. Manganese iron oxide ($MnFe_2O_4$) nanoparticle shows almost similar performance to that of Fe_2O_3. We observed that MnFe2O4 provides 96% tumor damage which is 3% more than the Fe_2O_3 NP. In case of healthy tissue, $MnFe_2O_4$ causes

5% more damage than the Fe_2O_3. Therefore, ferromagnetic nanoparticle (Fe_2O_3) outperforms gold and manganese iron oxide NPs. Therefore, ferromagnetic (Fe_2O_3) NPs outperforms in hyperthermia treatment.

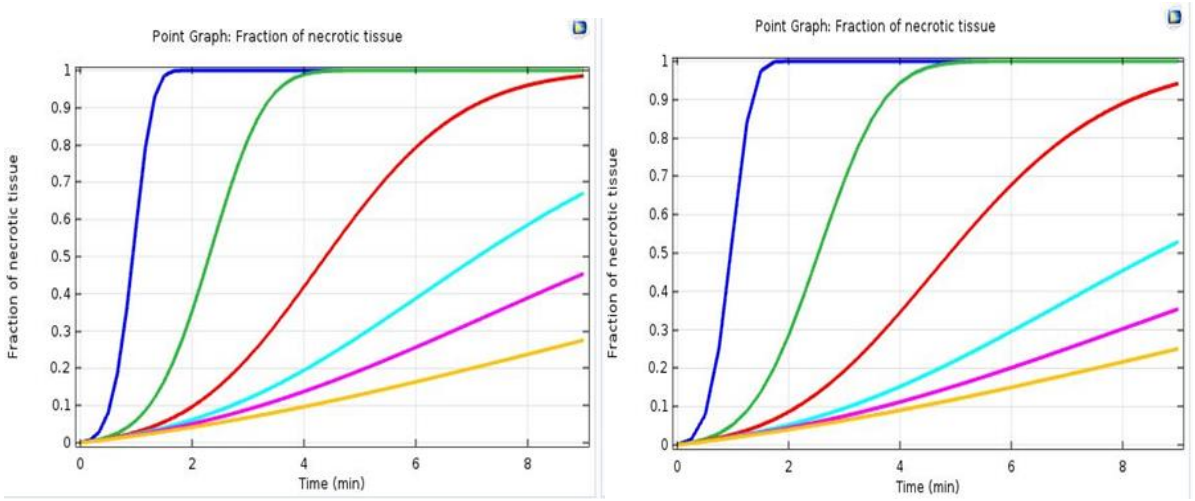

a) b)

Fig. 10 Point graph for damaged liver tissue with 433/915 MHz frequency:
a) before injecting NPs; b) after injecting NPs.

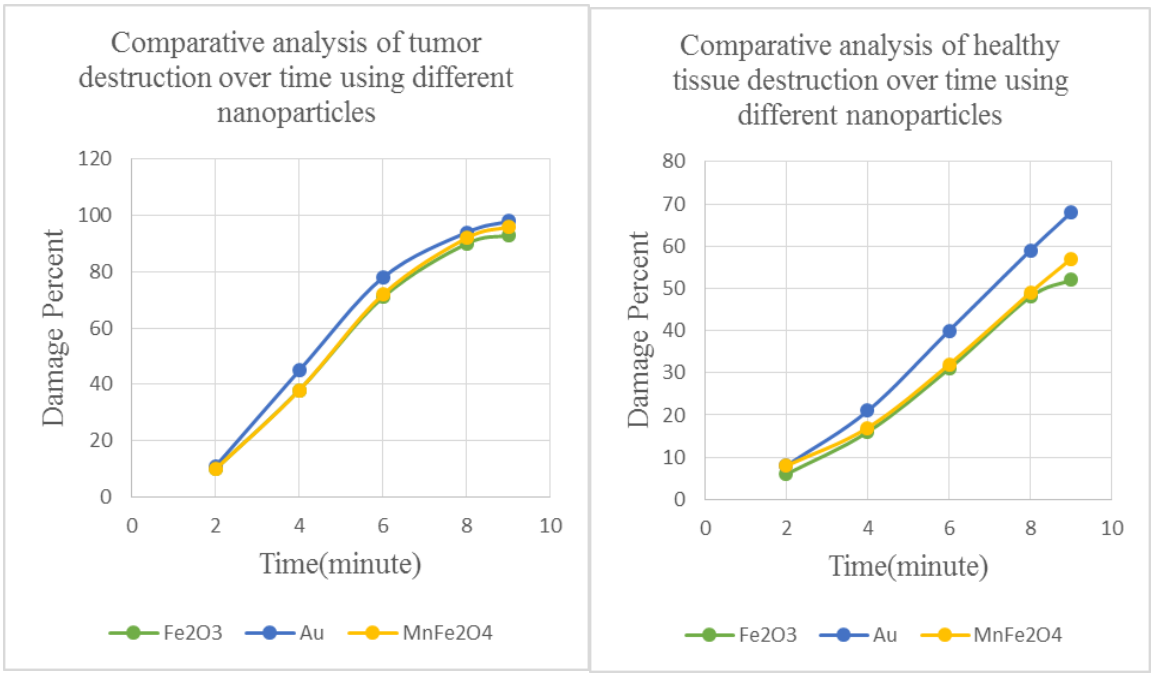

a) b)

Fig. 11 Performance analysis of different NPs for liver:
a) tumor damage; b) healthy tissue damage.

We have also analyzed the treatment procedure on human kidney, breast, and lung tissue while considering tumors on relevant tissue-mimicking phantoms. We have used the 433/915 MHz frequency and magnetic nanoparticle because of their better performance proved from the previous analysis.

Fig. 12a shows the percent of tumor damage over time on different human tissues caused by the microwave heating in absence of ferromagnetic NPs at 433/915 MHz. We see that the liver, kidney, breast, and lung tumors are fully damaged in 9, 6, 5 and 2 minutes of heating respectively. Fig. 12b represents the percent of tumor damage over time in presence of ferromagnetic NPs. The lung, breast, and kidney tumors are fully destroyed over 2, 5 and 6 minutes of heating respectively. Liver tumor damage is 95% within 9 minutes of heating.

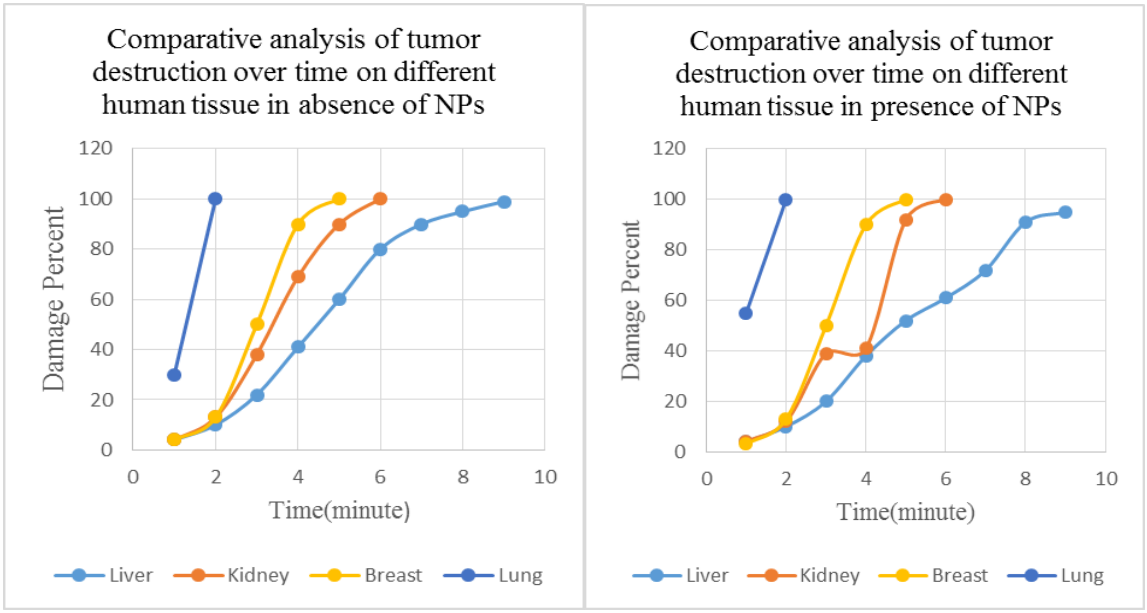

a) b)

Fig. 12 Comparative analysis of magnetic nanoparticle hyperthermia on the different human tissue: a) tumor damage without NP diffusion; b) tumor damage with NPs.

Fig. 13a illustrates the percent of healthy tissue damage on different human tissue caused by microwave heating.

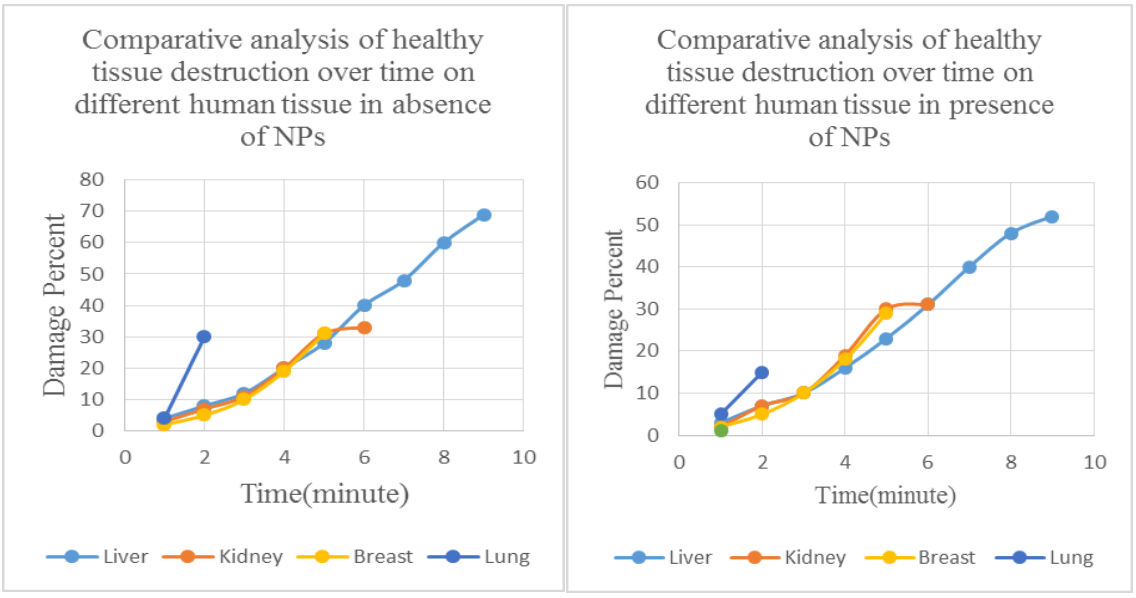

a) b)

Fig. 13 Comparative analysis of magnetic nanoparticle hyperthermia on different human tissue considering: a) healthy tissue damage without NP diffusion; b) healthy tissue damage with NPs.

The damage on healthy tissues surrounding the tumor of liver, kidney, breast, and lung is 69%, 33%, 31% and 30% for 9, 6, 5 and 2 minutes of heating respectively. Fig. 13b presents the percent of healthy tissue damage caused by the magnetic nanoparticle hyperthermia. The least damage of 15% occurs in lung tissue in 2 minutes of heating time and this is 15% less than that obtained with the heating procedure in absence of magnetic NPs. The highest damage of 52% is caused in the liver tissue in 9 minutes of heating which provides 17% less damage. Breast and kidney tissue damage percent is 29% and 31% over 5 and 6 minutes of heating respectively each providing 2% less damage to surrounding healthy tissue.

Conclusions

This research focuses on the improvement in Microwave coagulation therapy by incorporating ferromagnetic nanoparticles in the treatment domain. Firstly, we performed the simulation of microwave heating with and without diffusing the ferromagnetic nanoparticles in the targeted tumor region. Our study illustrates that the nanoparticles absorb the microwave radiation. Hence, the temperature is concentrated within the tumor thereby serving the purpose of destructing tumor cell with less hampering the healthy tissues. The same simulation is performed by varying microwave frequency and using different nanoparticles. The simulated result confirms that the 415/915 MHz frequency and ferromagnetic nanoparticle perform better in reducing healthy tissue damage. Moreover, the simulation was done for ablating lung, kidney and breast tumors using ferromagnetic nanoparticle and 415/933 MHz frequency value. In case of liver tumor ablation, the simulation findings are most promising providing 17% less damage of healthy tissue and maintaining healthy tissue temperature below 43 °C in most of the region. So, the findings of this research reveal that magnetic nanoparticle hyperthermia initiated by microwave heating can be effective in practical treatment cases by ensuring rapid ablation of the tumor while minimizing healthy tissue damage. The potential future directions this work can lead to is the experiment considering the effect of blood flow velocity and vessel location.

References

1. Abenojar E. C., S. Wickramasinghe, J. Bas-Concepcion, A. C. S. Samia (2016). Structural Effects on the Magnetic Hyperthermia Properties of Iron Oxide Nanoparticles, Progress in Natural Science: Materials International, 26, 440-448.
2. Ali S. M., A. K. Jha, S. Mahapatra, M. Panigrahi (2014). Cancer Detection Using Coagulation Therapy with Coaxial Antenna, Comsol International Conference, Bangalore, India, https://www.comsol.com/paper/download/210861/ali_paper.pdf (Last access December 04, 2019)
3. Blagoeva R., A. Nedev, V. Michailova (2017). An Approach to Modeling Drug Release from Polymersome Nanoparticles Based on PNIPAM-g-PEO Graft Copolymer, International Journal Bioautomation, 21(2), 179-188.
4. Deshan Y., J. M. Bertram, M. C. Converse, A. P. O'Rourke, J. G. Webster, S. C. Hagness, J. A. Will, D. M. Mahvi (2006). A Floating Sleeve Antenna Yields Localized Hepatic Microwave Ablation, IEEE Transactions on Biomedical Engineering, 53(3), 533-537.
5. Dutz S., R. Hergt (2014). Magnetic Particle Hyperthermia – A Promising Tumor Therapy, Nanotechnology, 25(45), 1-28.
6. Elkayal H. A., N. E. Ismail, M. Lotfy (2015). Microwaves for Breast Cancer Treatments, Alexandria Engineering Journal, 54(4), 1105-1113.
7. Huo X., U. M. Jow, M. Ghovanloo (2010). Radiation Characterization of an Intra-oral Wireless Device at Multiple ISM Bands: 433 MHZ, 915 MHZ, and 2.42 GHz, Annual International Conference of the IEEE Engineering in Medicine and Biology, 1425-1428.
8. Javidi M., M. Heydari, A. Karimi, M. Haghpanahi, M. Navidbakhsh, A. Razmkon (2014). Evaluation of the Effects of Injection Velocity and Different Gel Concentrations on

Nanoparticles in Hyperthermia Therapy, Journal of Biomedical Physics and Engineering, 4(4), 151-162.
9. Keangin P., T. Wessapan, P. Rattanadecho (2011). Analysis of Heat Transfer in Deformed Liver Cancer Modeling Treated Using a Microwave Coaxial Antenna, Applied Thermal Engineering, 31, 3243-3254.
10. Kobayashi T. (2011). Cancer Hyperthermia Using Magnetic Nanoparticles, Biotechnology Journal, 6(11), 1342-1347.
11. Krishnan K. M. (2010). Biomedical Nanomagnetics: A Spin through Possibilities in Imaging, Diagnostics, and Therapy, IEEE Transactions on Magnetics, 46(7), 2523-2558.
12. Pavel M., G. Gradinariu, A. Stancu (2008). Study of the Optimum Dose of Ferromagnetic Nanoparticles Suitable for Cancer Therapy Using MFH, IEEE Transactions on Magnetics, 44(11), 3205-3208.
13. Pearce J. A., J. R. Cook, S. Y. Emelianov (2010). Ferrimagnetic Nanoparticles Enhance Microwave Heating for Tumor Hyperthermia Therapy, Annual International Conference of the IEEE Engineering in Medicine and Biology, 2751-2754.
14. Salloum M., R. Ma, L. Zhu (2008). An *in vivo* Experimental Study of Temperature Elevations in Animal Tissue during Magnetic Nanoparticle Hyperthermia, International Journal of Hyperthermia, 24(7), 589-601.
15. Santos E. D., J. A. Green, N. Bhandari, A. Hong, P. Guitera, G. B. Fogarty (2015). Tangential Volumetric Modulated Radiotherapy – A New Technique for Large Scalp Lesions with a Case Study in Lentigo Maligna, International Journal Bioautomation, 19(2), 223-236.
16. Ward R. C., T. T. Healey, D. E. Dupuy (2013). Microwave Ablation Devices for Interventional Oncology, Expert Review of Medical Devices, 10(2), 225-238.
17. Yang D., M. Converse, D. Mahvi (2007). Expanding the Bio-heat Equation to Include Tissue Internal Water Evaporation during Heating, IEEE Transactions on Biomedical Engineering, 54(8), 1382-1388.

Kazi Mahdi Mahmud, B.Sc.
E-mail: utsha536@gmail.com

Mr. Kazi Mahdi Mahmud received his B.Sc. in Electronics and Communication Engineering (ECE) degree from Khulna University of Engineering & Technology (KUET), Khulna, Bangladesh, in 2018. His research interests are finite element modeling, microwave hyperthermia, and nanotechnology. Currently he is preparing for higher studies and research.

Assist. Prof. Md. Maruf Hossain Shuvo
E-mail: maruf.shuvo@ece.kuet.ac.bd

Md. Maruf Hossain Shuvo received his B.Sc. in Electronics and Communication Engineering (ECE) degree from Khulna University of Engineering & Technology (KUET), Bangladesh, in 2014. He is the University Gold Medalist and Prime Minister Gold Medalist. He received many awards including best paper awards at the international conferences in recognition of his research. After graduation, he has been working as a faculty member at ECE, KUET, since 2015, and currently works as an Assistant Professor. His research interests are medical imaging and analysis, finite element modeling, and computational biomedical engineering. He is a member of different professional societies and a reviewer of different conferences and journals.